

Modeling the Hard X-Ray Lag and Energy Spectrum of Cyg X-1

Xin-Min Hua^{1,2}, Demosthenes Kazanas¹, and Wei Cui³
submitted to *Astrophys. J.*, June 24, 1997

ABSTRACT

In an effort to model the observed energy spectrum of Cygnus X-1 as well as its hard X-ray lag by Comptonization in inhomogeneous clouds of hot electrons with spherical geometry and various radial density profiles we discovered that: 1) Plasma clouds with different density profiles will lead to different Comptonization energy spectra even though they have the same optical depth and temperature. On the other hand, clouds with different optical depths can produce the same energy spectra as long as their radial density distributions are properly chosen. Thus by fitting the energy spectrum alone, it is not possible to uniquely determine the optical depth of the Comptonization cloud, let alone its density structure. 2) The phase or time difference as a function of Fourier frequency or period for the X-rays in two energy bands is sensitive to the radial density distribution of the scattering cloud. Comptonization in plasma clouds with non-uniform density profiles can account for the long standing puzzle of the frequency-dependent hard X-ray lags of Cygnus X-1 and other sources. Thus simultaneously fitting the observed spectral and temporal X-ray properties will allow us to probe the density structure of the Comptonizing atmosphere and thereby the dynamics of mass accretion onto the compact object.

Subject headings: accretion— black hole physics— radiation mechanisms: Compton and inverse Compton— stars: neutron— X-rays

¹LHEA, NASA/GSFC Code 661, Greenbelt, MD 20771

²Universities Space Research Association

³Center for Space Research, MIT, Cambridge, MA 02139

1. Introduction

Much of our understanding of the physics and dynamics of accretion in X-ray binaries has been achieved mainly through the modeling and interpretation of their high energy photon spectra. The high energy emissions are believed to originate in the vicinity of the compact object and is considered to be due to the Comptonization of soft photons by the high temperature ($T_e \sim 10^9$ K) electrons heated by the dissipation of the accretion kinetic energy. This process has been studied extensively (e.g. Sunyaev & Titarchuk 1980; Hua & Titarchuk 1995) and model photon spectra in analytic forms have been used, quite successfully, to fit the observed spectra of accreting sources, in the energy range of a few to a few hundred keV. These fits can then provide the values of the Thomson optical depth τ_0 and the temperature T_e of the hot electrons. While the parameters so obtained are widely accepted as the true indication of the physical conditions prevailing in the region under consideration, one should keep in mind that the analytical formulas derived are based on several approximations. Hua & Titarchuk (1995) showed that in order for the analytical formulas to be valid, the optical depth τ_0 and the electron temperature T_e must be within certain limits and the initial distribution of source photons must satisfy certain requirements. Furthermore, the analytical treatment can only be applied to the simplest geometries, typically spheres or disks with uniform temperature and density. Obviously, these requirements are not realistic in most situations.

For example, Skibo & Dermer (1996) and Ling et al. (1997) have shown that for some of the observed energy spectra, two zone models of different temperatures can significantly improve the energy spectral fits. Along the same lines, Kazanas et al. (1997, hereafter KHT), motivated by considerations of the accretion dynamics and the variability of the observed light curves as manifest in the form of power spectra (Miyamoto et al. 1992, Cui et al. 1997b), introduced a model consisting of an extended Comptonizing atmosphere in spherical geometry, with density profiles r^{-1} or $r^{-3/2}$, where r is the distance from the center of the spherical clouds. Hua et al. (1997, hereafter HKT) further showed that the hard X-ray time lags and the sources' coherence functions, derived from observations of X-ray binaries by Ginga (Miyamoto et al. 1991, Vaughan & Nowak, 1997), and also by more recent observations by RXTE (Cui et al. 1997b) are

consistent with the inhomogeneous models introduced by KHT and inconsistent with the uniform ones.

These more realistic models have more adjustable parameters and before they can be used to interpret the observational data, the question arises as to how the energy spectra resulting from such models depend on these extra parameters. An additional question is whether there exist any observational tests which can provide information concerning the inhomogeneity present in these more general models. The purpose of the present paper is to provide answers to these questions.

In §2, we show how the radial density profiles of scattering clouds with a given optical depth and temperature can affect the emergent energy spectra. In §3, we provide an example of spectral fitting of the Cygnus X-1 data obtained in combination by CGRO/BATSE and RXTE/PCA using model spectra corresponding to configurations of different density profiles. In §4, we show that X-ray time lags corresponding to these different models are sufficiently different to serve as a discriminator of these models, thus giving preference to a particular class of inhomogeneous model. In §5, we present a simple analytic model which provides a transparent account of the numerical results. Finally, in §6 we provide a summary and conclusions of our results and we discuss the implication of these models for the interpretation of observational data.

2. The Effects of The Density Profile on The Energy Spectrum

In the present study we concentrate on the Comptonization process in hot electron clouds with density profiles of the form

$$n(r) = \begin{cases} n_i & \text{for } r \leq r_1 \\ n_1(r_1/r)^p & \text{for } r_2 > r > r_1 \end{cases} \quad (1)$$

where p is a free parameter; r is the radial distance from the center of a spherical cloud; r_1 and r_2 are radii of the inner and outer edges of the extended non-uniform “atmosphere” respectively. The central core is assumed to be uniform and its density is n_i , which may not necessarily equal to n_1 .

For illustration purposes, we have calculated the energy spectra emerging from clouds with the same total optical depth $\tau_0 = 1$ and electron temperature $kT_e = 100$ keV but different density profiles, namely $p = 3/2, 1$ and 0 in Eq. (1). The first two pro-

files represent the dynamically more plausible free-fall ($p = 3/2$) density distribution such as implied by the advection-dominated accretion model suggested by Narayan & Yi (1994) and the accretion induced by the sort of radiative viscosity ($p = 1$) suggested by KHT. For the uniform profile ($p = 0$), traditionally used in spectral fitting because of its mathematical simplicity, we further assume that it has an electron density of the order $10^{16-17} \text{ cm}^{-3}$ and a size of the order $\sim 10^{-3}$ light second, typical of the values thought appropriate for the conditions in the vicinity of the compact object in galactic accreting sources. For the other two profiles, both central cores have radius $r_1 = 1.0 \times 10^{-3}$ light seconds. In the absence of detailed knowledge of this innermost part of accreting cloud, we simply assume it has uniform density n_i such that its Thomson optical depth $\approx \tau_0/3$.

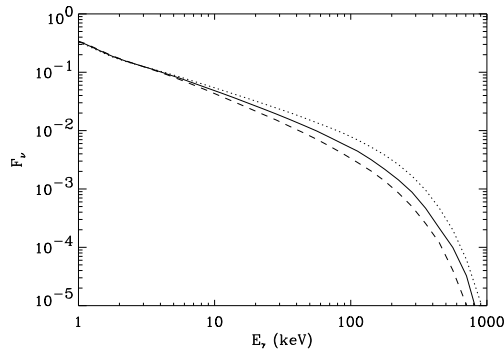


Fig. 1.— Energy spectra resulting from Comptonization in clouds with different density profiles. The clouds have the same optical depth $\tau_0 = 1$ and plasma temperature $kT_e = 100$ keV. The spectra are from clouds with uniform (dotted), $p = 1$ (solid) and $p = 3/2$ (dashed curve) density profiles respectively.

Model energy spectra obtained using the Monte Carlo code of Hua (1997), developed to deal with photon propagation and Compton scatterings in inhomogeneous media, for conditions appropriate for these density profiles are shown in Figure 1. It is seen that although the emissions are from clouds with the same optical depth and plasma temperature, their spectra are significantly different from each other. In general, for the same τ_0 , T_e , r_1 , n_1 and n_i in Eq. (1), the greater the density gradient represented by p , the softer the emergent photon energy spectrum for a given total Thomson depth τ_0 . This is because photons propagating in media with a density gradient

are in an anisotropic environment – the outward scatterings have longer mean free path than the inward ones. Consequently, clouds with greater density gradient are more difficult to trap the photons, leading to softer energy spectra.

3. Modeling the Energy Spectrum of Cyg X-1

The above discussion indicates that the optical depth and plasma temperature alone are not sufficient to determine the spectrum due to the Comptonization process. Clouds with the same optical depth and temperature can lead to different Comptonization spectra if they have different density distributions. On the other hand, clouds with different optical depths or temperature can lead to the same photon spectrum as long as their density profiles are properly chosen. This can be clearly seen in the following example of spectral fitting in which three photon spectra resulting from clouds with the same temperature but different optical depths and density profiles fit equally well a given set of observational data. The data are taken from Table 2 of Ling et al. (1997), which tabulates the spectrum of the blackhole candidate Cyg X-1 at its γ_0 state observed in late 1993. Ling et al. (1997), using a Monte Carlo simulation of Comptonization in uniform density clouds, obtained a best-fit model corresponding to a spherical cloud with optical depth $\tau_0 = 0.435$ and temperature $kT_e = 107.7$ keV.

The spectrum was obtained by Comptonization of seed photons from a black body distribution of temperature $kT_e = 0.5$ keV. The source of photons was considered to lie outside the hot electron cloud and to be injected radially inward as suggested by Skibo & Dermer (1995). Here we re-fit the same data using a slightly different model with $\tau_0 = 0.5$, $kT_e = 100$ keV and source photons at $kT_0 = 0.2$ keV injected isotropically at the cloud center. The cloud is assumed to be uniform as in the previous fitting. The spectrum resulting from such a model is displayed in Figure 2 (dotted curve) together with the data points. The reduced χ^2 value is 10.3 with 11 degrees of freedom, not as low as the one obtained by Ling et al. (1997) but still perfectly acceptable.

In the same figure, we also display the Monte Carlo calculated spectra resulting from two other models which have the same plasma temperature $kT_e = 100$ keV but different optical depths τ_0 and non-uniform density profiles. One of them is a cloud with density

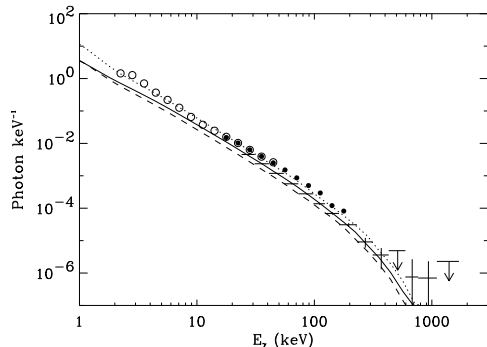


Fig. 2.— Three calculated energy spectra which fit equally well the Cyg X-1 data (crosses) in its γ_0 state observed by CGRO/BATSE in 1994 (Ling et al. 1997). These spectra result from Comptonization in clouds with the same temperature but different optical depths and density profiles. The dotted and dashed curves are slightly displaced to separate the otherwise nearly identical curves. Also plotted are RXTE/PCA (circles) and HEXTE (dots) data from the same source observed during its high state in 1996 (Cui et al. 1997a).

profile parameter $p = 1$ and $n_1 = 4.35 \times 10^{16} \text{ cm}^{-3}$. Its inner core has a uniform density and a radius $r_1 = 10^{-4}$ light second with a Thomson optical depth $\tau_1 = 0.2$. The total optical depth of the cloud is 1 and the energy spectrum resulting from Comptonization in such a cloud is displayed in Figure 2 as the solid curve. The other model is a cloud with $p = 3/2$ and $n_1 = 1.594 \times 10^{17} \text{ cm}^{-3}$. Its uniform inner core has the same radius but a Thomson optical depth $\tau_1 = 0.07$. The total optical depth of the cloud is 0.7 and the energy spectrum from such a cloud is displayed in Figure 2 as the dashed curve. It is seen that over the energy range from 20 to 200 keV, these spectra are almost identical to the dotted curve. In fact, the χ^2 values are 7.8 and 8.1 respectively (with 8 degrees of freedom). In other words, these two models are as good as the uniform one insofar as the spectral fits are concerned.

Since these spectra were produced by a Monte Carlo calculation, a few words about its statistical errors are in order. Each of the spectra was obtained by following 8×10^6 photons. By generating several such spectra under the same conditions but with a different initial random number seeds and by fitting the spectra to the same data, we were able to esti-

mate the statistical uncertainty of the calculation. It was found that the standard deviation of the χ^2 value introduced by the Monte Carlo statistics is less than 2, which is small compared to the χ^2 values obtained. This justifies the conclusion about the goodness of the fits.

In Fig. 2 we also plotted the PCA (circles) and HEXTE (dots) data covering an energy range 2–200 keV from RXTE observations of Cyg X-1 in its 1996 high state (Cui et al. 1997a). By definition, the soft X-ray ($\lesssim 10$ keV) flux is high in the high state, but the hard flux is low. Such a distinct anti-correlation between the soft and hard bands was confirmed by the simultaneous monitoring of Cyg X-1 with the ASM/RXTE and BATSE (Cui et al. 1997a, Zhang et al. 1996). Cyg X-1 in the γ_0 state, as defined by Ling et al. (1997), showed a similar BATSE flux. So it might have been in the high state as well in 1994. Unfortunately, no simultaneous soft X-ray coverage was available then to confirm it. On the other hand, the remarkable similarity in the observed X-ray spectral shape, as is evident from the figure, between these two observations 2.5 year apart also seems to suggest a common origin. If so, the results would imply that the high state spectrum of Cyg X-1 (and perhaps the high state itself) is quite stable, except for a slight shift in the normalization (part of which can be attributed to the uncertainty in the cross calibration between the RXTE instruments and BATSE).

4. Hard X-Ray Time Lag of Cyg X-1

Although clouds with different density profiles can produce the same energy spectrum, at least over a given energy range, as long as they have properly chosen τ_0 and T_e , KHT and HKT have shown that the time-variation properties of the sources are sensitive to the density distribution of the Comptonizing atmosphere and therefore they can be used to distinguish the models of different density profiles. In fact, the inhomogeneous density profile models were conceived by KHT in order to explain the observed temporal properties such as power spectral density (PSD) and hard X-ray phase or time lags. In Figure 3, we show the time lags of the X-ray emission as a function of Fourier period (see e.g. van der Klis et al. 1987) resulting from the three model clouds which were used to produce the energy spectra shown in Figure 2. These were obtained using the Monte Carlo code by collecting the escaping photons according to

their arrival time to the observer as well as their energy. The photons were collected in the two energy bands 15.8–24.4 and 1.2–5.75 keV in order to be directly compared to the observational data obtained by Ginga (Miyamoto et al. 1988). In each energy band, the photons were collected into 4096 bins over 16 seconds, each 1/256 seconds in length. The light curves so obtained were then used to calculate the time lags of the emission in the 15.8–24.4 keV band with respect to that in the 1.2–5.75 keV band. The time lag resulting from the uniform cloud (dotted curve) is obtained by further assuming the cloud has a density $n = 10^{16} \text{ cm}^{-3}$. It is seen that the lag decreases below the period ~ 0.005 second but becomes constant ≈ 2 ms above it. This is because for emission from such a cloud, the hard X-ray lags are due to scatterings in a region with a mean free time of the order $0.3/n\sigma_{\text{T}}c \simeq 1.5$ ms (Hua & Titarchuk, 1996). The magnitude of the time lag reflects this characteristic time.

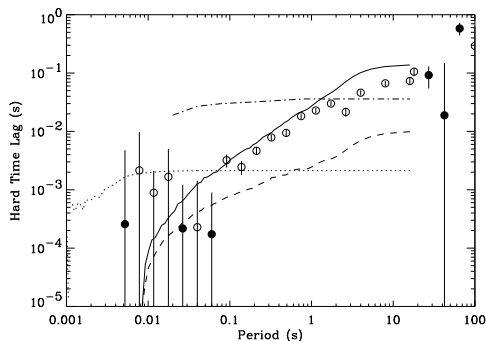


Fig. 3.— The time lags of hard X-rays (15.8–24.4 keV) with respect to soft ones (1.2–5.7 keV) resulting from Comptonization in the same clouds that produce the energy spectra shown in Figure 2. The dotted, solid and dashed curves, as in Figure 2, represent the density profiles $p = 0, 1$ and $3/2$ respectively. The time lag between the same energy bands based on Ginga data from Cyg X-1 (Miyamoto et al. 1988) are also plotted in the figure.

On the other hand, the time lag resulting from the cloud with $p = 1$ density profile (solid curve) has a linear dependence on the Fourier period ranging from 0.03 second up to ~ 3 second. There is a cutoff at the periods below the range due to the finite time resolution of our calculation. At periods $P \gtrsim 4$ seconds the curve levels off, indicating that the time lag of hard

X-ray reaches its maximum of ~ 0.1 second. This is because the lags in this case are due to scatterings in a region with densities ranging from $\sim 10^{16}$ to 10^{12} cm^{-3} . In addition, the probabilities for photons to scatter in each decade of density are equal (KHT). Correspondingly, the scattering mean free time spans a range of four orders of magnitude. As a result, the time lags also span a range of four orders of magnitude, and the level-off period roughly indicates the size of the cloud, which is 1 light second in this case. The time lag resulting from the cloud with $p = 3/2$ density profile is also plotted in Figure 3 (dashed curve). It is seen that dependence of lag on period is weaker and the maximum time lag is only $\sim 10^{-2}$ second, indicating that although the cloud extends to a radius of ~ 1 light second, because of the steep density gradient, there is virtually no photon scattering beyond a radius $\sim 10^{-2}$ light second. A calculation based on the density profile of Eq. (1) indicates that the optical depth of the cloud for $r > 10^{-2}$ light second is $\sim 7.5\%$ of the total depth for $p = 3/2$, while in the case of $p = 1$, the corresponding percentage is 40%.

Also plotted in Figure 3 is the time lag observed from Cyg X-1 between the same energy bands by Ginga (Miyamoto et al. 1988). It is seen that, qualitatively, the nearly linear dependence of time lag on Fourier period is best fitted by the curve representing the cloud with $p = 1$ density profile. The curve for the cloud with $p = 3/2$ density profile, because of its weaker dependence on the Fourier period, obviously does not provide as good a fit to the data and could be considered excluded for this specific data set. It is also obvious that a uniform cloud model can be excluded, a conclusion reached also by Miyamoto et al (1988) by comparing the time lag obtained based on the analytic formula of Payne (1980) for a uniform cloud. The latter time lag corresponding to a density $n = 10^{16} \text{ cm}^{-3}$ is plotted in the figure as a dash-dotted curve. The difference between the analytic curve and Monte Carlo result (over one order of magnitude) is mainly due to the relativistic electron temperature and small optical depth as explained in Hua & Titarchuk (1996).

However, the Ginga data presented in fig. 3 were obtained in August 1987, when Cyg X-1 was in its low state. Therefore, it may be considered inappropriate to compare them with the calculated time lags based on the cloud configuration used to fit the energy spectrum of the 1993 observation, when the source

was in its high (soft) state. On the other hand, as pointed out in §3, the RXTE observations of Cyg X-1 in 1996 (Cui et al. 1997a) not only provide data in its high (soft) state but also data whose spectrum is similar to that of the 1993 observation. The time lags of the RXTE observation were reported in Cui et al. (1997b). As an example, here we use their results from observation #6 for comparison, when the source was in its high (soft) state while the other two reported (# 3 and # 15) were during the transitions. The Fourier period dependence of the time lag of the energy band 13 – 60 keV with respect to 2 – 6.5 keV is plotted in Figure 4 with the data points re-grouped into logarithmically uniform bins in Fourier period. Again, the linear dependence of the lag on the Fourier period in the range $\sim 0.03 - 3$ second is evident. The lags between the same energy bands calculated for the three model clouds described above are also plotted in the figure. The shapes of the curves are similar to those in figure 3, but the magnitudes of the lag are slightly smaller, clearly because of the smaller gap between the reference energy bands in this case. Obviously, the cloud with $p = 1$ is again favored by the observation.

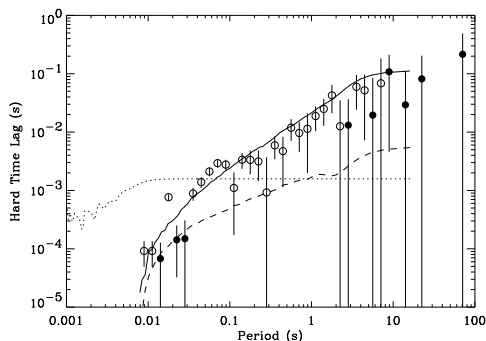


Fig. 4.— The time lags of hard X-rays (13 – 60 keV) with respect to soft ones (2 – 6.5 keV) resulting from Comptonization in the same clouds that produce the energy spectra shown in Figure 2. The dotted, solid and dashed curves, as in Figure 2, represent the density profiles $p = 0, 1$ and $3/2$ respectively. The time lag between the same energy bands based on RXTE data from Cyg X-1 (Cui et al. 1997b) are also plotted in the figure.

In addition to these Cyg X-1 data, Ginga data from GX399-4 during its very high state (Miyamoto et al. 1991) also show a nearly linear dependence of the hard

X-ray time lags on the Fourier period over the range from ~ 0.1 to $\gtrsim 10$ seconds. The lags at low frequencies could be as large as ~ 1 second. More recently, CGRO/OSSE data from the source GRO J0422+32 (Grove et al 1997) show a similar dependence for photons in the energy band 75 – 175 keV with respect to those in the band 35 – 60 keV over the Fourier frequency range 0.03 – ~ 10 Hz. The time lag reaches ~ 0.3 second and levels off at ~ 0.03 Hz. Therefore we have reason to believe that the nearly linear time lag dependence on Fourier period is a common phenomenon shared by many accreting compact objects.

The above comparisons for the Cyg X-1 data, qualitative as they are, show that by detailed fitting to the observed time lag as a function of frequency or period, one can determine the density structure of the Comptonizing cloud. More importantly, they show that, if in addition simultaneous spectral data are available, the combined analysis of spectral and temporal data from the same source can uniquely determine the physical size, density profile as well as optical depth, temperature of the plasma cloud responsible for the X-ray emissions. We are planning to do more detailed data fitting to the energy spectra, time lag and other properties observed simultaneously from Cyg X-1 and other sources.

5. Discussion

The difference of the time lag curves resulting from Comptonization in clouds with uniform and non-uniform density profiles, in particular the one with $p = 1$, can be better understood if we examine the detailed form of their corresponding high energy light curves in response to an instantaneous input of soft photons at their center. In KHT, it was shown that the light curve resulting from Comptonization in a uniform cloud is exponential in time while that from a cloud with $p = 1$ density profile has a power law shape, with power index close to one which decreases with increasing total Thomson depth and photon energy. In both cases there is a cutoff corresponding to the time scale characteristic of the photon escape time from the system β . These light curves can be approximated very well analytically by the Gamma distribution function

$$g(t) = \begin{cases} t^{\alpha-1} e^{-t/\beta}, & \text{if } t \geq 0; \\ 0, & \text{otherwise,} \end{cases} \quad (2)$$

where t is time; $\alpha > 0$ and $\beta > 0$ are parameters determining the shape of the light curves.

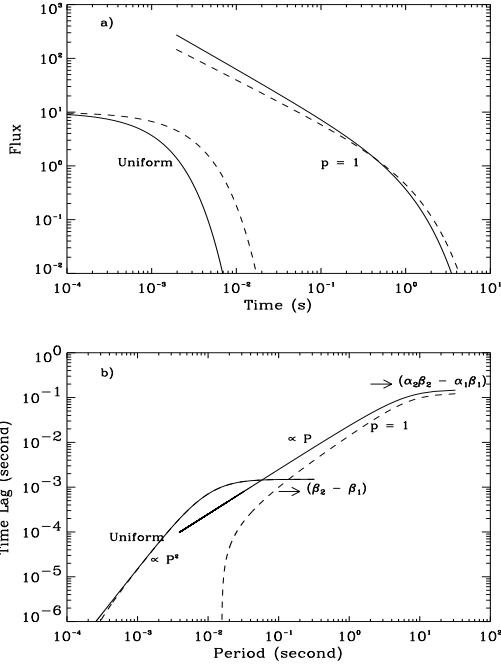


Fig. 5.— (a) Two pairs of light curves corresponding to two sets of values of α and β in Eq. (2). The pair with $p = 1$ represents the light curves from a cloud with $1/r$ density profile, the other pair from a uniform one. The solid curves correspond to the light curves in the lower energy bands. (b) The time lag based on Eq. (5) between the two curves in each pair in (a). The dashed curves are time lags obtained by numerical Fourier transformation with finite time resolution.

The light curve from a uniform electron cloud corresponds to $\alpha = 1$ so that the Gamma distribution function reduces to an exponential. Because the cloud in this case is assumed to be confined to the vicinity of the compact object, the corresponding value for β is of order of 10^{-3} sec. The cloud with the $p = 1$ density profile under consideration is much more extended spatially, with its outer radius at ~ 1 light second, corresponding to $\beta \sim 1$ second, and with a value for α small compared to 1. The Fourier transformation of $g(t)$ is

$$G(\omega) = \frac{\Gamma(\alpha)\beta^\alpha}{\sqrt{2\pi}}(1 + \beta^2\omega^2)^{-\alpha/2}e^{i\alpha\theta}. \quad (3)$$

where $\Gamma(x)$ is the Gamma function; $\omega = 2\pi/P$ is the Fourier frequency and θ is the phase angle that we are interested in and

$$\tan \theta = \beta\omega. \quad (4)$$

If we consider two light curves in two energy bands distinguished by the different values of α and β , say α_1, β_1 and α_2, β_2 , the time lag between them will be given by their phase lag θ divided by the corresponding Fourier frequency ω , i.e.

$$\delta t = \frac{1}{\omega} [\alpha_2 \arctan(\beta_2\omega) - \alpha_1 \arctan(\beta_1\omega)] \quad (5)$$

For large periods P or $\beta_1\omega, \beta_2\omega \ll 1$, δt approaches the constant $\alpha_2\beta_2 - \alpha_1\beta_1$. On the other hand, for small P , $\delta t \simeq (\alpha_2 - \alpha_1)P/4$. The transition from latter to the former occurs at $\beta\omega \sim 1$ or $P \sim 2\pi\beta$. In our model for $p = 1$ density profile, β_1 and $\beta_2 \sim 1$ second. This explains what we see in Figures 3 and 4, namely for $P \lesssim$ a few seconds, $\delta t \propto P$ and the curve levels off for large P . On the other hand, for the case of uniform cloud, $\alpha_1 = \alpha_2 = 1$; β_1 and $\beta_2 \sim 1$ ms (§4). As a result, for large periods P , δt approaches the constant $\beta_2 - \beta_1$, which is of the order 1 millisecond. For small P , $\delta t \propto (1/\beta_1 - 1/\beta_2)P^2$. The transition occurs at $P \sim 2\pi\beta \simeq 0.006$ second.

In Figure 5a, we plot two pairs of light curves, one with $\alpha_1 = 0.1, \alpha_2 = 0.2, \beta_1 = 1$ and $\beta_2 = 1.25$, the other with $\alpha_1 = \alpha_2 = 1.0, \beta_1 = 0.001$ and $\beta_2 = 0.0025$. The former represents the light curves resulting from the cloud with $p = 1$ density profile while the latter from a uniform one. The time lags between these two pairs of light curves are presented in Figure 5b. It is seen that the light curve parameters α and β determine the shape of the time lag curve: For $\alpha = 1$, or pure exponential light curves, the time lag is proportional to P^2 for small Fourier period P and turns to constant for large P . For $0 < \alpha < 1$, the time lag is proportional to P for small P and turns to constant for large P . In both cases, the level-off point is $P \approx 2\pi\beta$. However, the time lag resulting from the exponential light curves has no portion linear in P . Thus the existence of a linear portion in the time lag curves obtained from observations clearly favors the power law light curve. From KHT, we know that power law light curve is a signature of the non-uniform density distribution of the source and the values of α and β are closely related to the physical size and density distribution of the source cloud.

Thus, under the assumptions of the present calculations (i.e. Comptonization as the main process

of high energy emission, uniform temperature, non-uniform density) the time dependence of the photon flux, or light curves, at various energies can be used to map the radial density distribution of the hot electron Comptonizing cloud. This fact provides the possibility of deconvolution of the density structure of these clouds through timing analysis of their light curves.

6. Conclusions

1) For a given total Thompson depth of the Comptonization cloud, τ_0 , the electron density distribution can significantly affect the emergent spectrum. Consequently, clouds of the same depth τ_0 and electron temperature T_e can lead to different Comptonization spectra depending on their density distributions. On the other hand, clouds with different optical depths or temperature can lead to the same photon spectrum as long as their density profiles are properly chosen. In other words, analysis of energy spectra alone cannot determine the optical depth τ_0 of the cloud, if its density structure is unknown. Consequently, all the τ_0 and T_e values obtained by the traditional way of fitting analytically or numerically calculated energy spectra with observational data are not the true reflection of these properties but only indicate the effective values of a uniform plasma cloud.

2) The phase or time differences between X-rays in two energy bands as functions of the Fourier frequency or period can provide additional, independent diagnostics of the light curve shapes and thereby of the density structure of the scattering medium. This is because the phase or time differences reflect the shape of the light curves, which in turn map the density profiles of the clouds. In the framework of Comptonization, the phase or time lags depend only on the physical size and density of the scattering medium. Therefore the information they provide is independent of possible alternative influences other than Compton scattering; such influences would generally afflict the most common test of variability, namely the PSD. For example, in timing analysis of the light curves in terms of shots, the corresponding PSDs depend on the shot distribution, morphology and modulation of their rate of injection. The time lag analysis is immune of all these influences.

Therefore, combined analysis of spectral and temporal properties can yield knowledge not only about optical depth and plasma temperature but also about the physical size and density structure of the plasma

clouds. When simultaneous observation of energy spectra and time variability, especially the time lags, from a source are available, fitting of data in the combined spectral and temporal domains such as those presented in this study, will provide less ambiguous information about these physical properties that are important in the understanding of the the dynamics of mass accretion onto the compact object.

The authors would like to thank J.C. Ling, J.E. Grove, S.N. Zhang and W. Focke for useful discussions.

REFERENCES

- Cui, W. et al. 1997a, ApJ, 474, L57
 Cui, W. et al. 1997b, ApJ, 484 in press (astro-ph/9702073)
 Grove, J. E. et al. 1997, ApJ, in preparation
 Hua, X.-M. 1997 Computers in Physics, in press
 Hua, X.-M. & Titarchuk, L. 1995 ApJ, 449, 188
 Hua, X.-M. & Titarchuk, L. 1996 ApJ, 469, 280
 Hua, X.-M., Kazanas, D. & Titarchuk, L. 1997 ApJ, 482, L57 (HKT)
 Kazanas, D., Hua, X.-M. & Titarchuk, L. 1997 ApJ, 480, 735 (KHT)
 Ling, J. C. et al., 1997, ApJ, 484, 375
 Miyamoto, S. et al., 1988, Nature, 336, 450
 Miyamoto, S. et al., 1991, ApJ, 383, 784
 Miyamoto, S. et al., 1992, ApJ, 391, L21
 Narayan, R. & Yi, I., 1994, ApJ, 428, L13
 Skibo, J. G. & Dermer, C. D., 1995, ApJ, 455, L25
 Sunyaev, R. A. & Titarchuk, L. G., 1980, A&A, 86, 121
 Titarchuk, L. G., 1994, ApJ, 434, 570
 van der Klis, M. et al., 1987, ApJ, 319, L13
 Vaughan, B. A. & Nowak, M. A. 1997 ApJ, 474, L43
 Zhang, S. N., Harmon, B. A., Paciesas, & Fishman, G. J. 1996, IAU Circ. 6405

This 2-column preprint was prepared with the AAS L^AT_EX macros v4.0.